Applied Surface Science 256 (2010) 5069–5075

Contents lists available at ScienceDirect

Applied Surface Science

journal homepage: www.elsevier.com/locate/apsusc

Structural and electrical characterization of the nickel silicide films formed at 850 °C by rapid thermal annealing of the Ni/Si(1 0 0) films

G. Utlu[a,*], N. Artunç[a], S. Budak[b], S. Tari[c]

[a] Ege University, Faculty of Science, Department of Physics, 35100 Bornova, Izmir, Turkey
[b] Department of Electrical Engineering, Alabama A&M University, Normal, AL 35762, USA
[c] İzmir Institute of Technology, Department of Physics, 35430 Urla, Izmir, Turkey

ARTICLE INFO

Article history:
Received 2 October 2009
Received in revised form 8 March 2010
Accepted 13 March 2010
Available online 19 March 2010

Keywords:
Nickel di-silicide
Rapid thermal annealing (RTA)
Thickness-dependent silicide formation
Sheet resistance
XRD
RBS
SEM
X-SEM and AFM techniques

ABSTRACT

Nickel di-silicide formation induced by RTA process at 850 °C for 60 s in the Ni/Si(1 0 0) systems are investigated as a function of the initial Ni film thickness of 7–89 nm using XRD, RBS, SEM, X-SEM and AFM. Based on the XRD and RBS data, in the silicide films of 400–105 nm, NiSi and $NiSi_2$ silicide phases co-exist, indicating that Ni overlayer is completely transformed to NiSi and $NiSi_2$ silicide phases. SEM reveals that these films consist of large grains for co-existence of $NiSi_2$ and NiSi phases, separated from one another by holes, reflecting that $NiSi_2$ grows as islands in NiSi matrix. These films have low sheet resistance, ranging from 1.89 to 5.44 Ω/□ and good thermal stability. For thicknesses ≤ 80 nm RBS yields more Si-rich silicide phases compared to thicker films, whereas SEM reveals that Si-enriched silicide islands with visible holes grow in Si matrix. As the film thickness decreases from 400 to 35 nm, AFM reveals a ridge-like structure showing a general trend of decreasing average diameter and mean roughness values, while sheet resistance measurements exhibit a dramatic increase ranging from 1.89 to 53.73 Ω/□. This dramatic sheet resistance increase is generated by substantial grain boundary grooving, followed by island formation, resulting in a significant phase transformation from $NiSi_2$-rich to Si-rich silicide phases.

1. Introduction

In recent years nickel silicides, intermetallic compounds of silicon and nickel, have been proposed as candidates for replacing aluminum alloys for applications in very large-scale integrated circuits (VLSI) [1–4] and in ultra large-scale integrated circuits (ULSI) [3–5], because they show metallic behavior with low electrical resistivity, high electro-migration resistance, high thermal stability and resistance to acids [1,4]. Nickel silicides can be formed by solid-state reaction of Si and thin nickel films, deposited on Si wafer, at a temperature well below the eutectic temperature of the system [6–12], although other techniques such as explosive silicidation [13], reactive deposition [14] and ion implantation [15–17] can also be used. In solid-state reaction technique, silicide formation is induced by thermal annealing in Ni/Si thin film system, using various annealing techniques such as isothermal furnace annealing, rapid thermal annealing (RTA), laser and electron beam annealing [6]. It has been reported that the developed phases of nickel silicide (Ni_2Si, NiSi and $NiSi_2$) are temperature-dependent and formed by different growth mechanisms [6–12]. Ni_2Si, NiSi and $NiSi_2$ form in the temperature ranges of 200–350, 350–750 and 750–1000 °C, respectively [6–12]. Unlike Ni_2Si and NiSi formation, which are diffusion controlled processes, $NiSi_2$ formation has been reported to be nucleation controlled [4,6,7,18]. Furthermore, the growth-dynamics of different silicide phases has been reported to be dependent on the amounts of Ni and Si atoms available for the silicide formation due to the film thickness for a given annealing temperature and time for the case of the thin film couples [6,19].

NiSi is thermally stable only up to the temperatures of about 650–700 °C, thereafter high resistivity phase $NiSi_2$ starts to nucleate [6–12,18]. NiSi has been also reported to agglomerate during the silicidation process at temperature as low as 600 °C [6–12]. This thermal instability of NiSi is a drawback in applying it to CMOS manufacturing and integration process [3,12,20–22]. However, nickel di-silicide ($NiSi_2$) formed from the low resistivity phase NiSi has the lowest lattice mismatch to Si and shows good epitaxial growth on Si [20,23]. $NiSi_2$ exhibits good thermal stability up to high temperatures of about 1000 °C. $NiSi_2$ loses adhesion to Si near its melting point of ~993 °C [21], thereafter it starts to agglomerate with grain boundary grooving, followed by grain separation and formation of silicide islands, resulting in a dramatic increase in sheet resistance [20,24–27]. This thermal instability is the main drawback which restricts its applications in deep submicron devices. More importantly, for the films with thicknesses

* Corresponding author. Tel.: +90 232 388400 2361; fax: +90 232 3881036.
E-mail address: gokhan.utlu@ege.edu.tr (G. Utlu).

0169-4332/$ – see front matter © 2010 Elsevier B.V. All rights reserved.
doi:10.1016/j.apsusc.2010.03.062

≤50–60 nm, $NiSi_2$ agglomeration takes place at even lower temperatures than normally expected value of about 1000 °C [25,28]. Therefore, thickness dependence of the thermal stability of $NiSi_2$ thin film is crucial criterion for deep submicron devices. Apart from this, with the continuous scaling down of devices, silicide film thickness (especially ≤50 nm) becomes an important parameter, which controls first stages of the silicide formation and other phenomena such as nucleation, lateral growth, stress and texture [28–30]. Therefore, it is very important to understand and control the silicide formation as function of the film thickness for a fixed annealing temperature.

In this study, therefore, the first aim is to deposit Ni thin films, with thicknesses ranging from 7 to 89 nm, onto n-type Si(1 0 0) substrate by thermal evaporation technique, and then to anneal these Ni/Si bilayers by RTA process for 60 s at 850 °C so as to synthesize nickel di-silicide ($NiSi_2$) films by solid-state reaction technique. The second aim is to investigate the effects of the initial Ni film thickness on the Ni–Si silicide formation induced by rapid thermally annealing in the Ni/Si(1 0 0) systems using XRD, RBS, SEM, X-SEM, AFM and sheet resistance measurement techniques. The correlation of Ni–Si silicide formation with its electrical and morphological properties is also established.

2. Experimental details

In this study, firstly Ni thin films were deposited on n-type Si(1 0 0) substrate with resistivity of 1–10 Ω cm by thermal evaporation of Ni wire of purity 99.99% with a diameter of 1.0 mm, using an Edward high vacuum coater system with the base pressure of about 1×10^{-6} Torr. The silicon wafers were cut into small pieces of 45 mm × 20 mm size, so as to deposit a Ni film of 15 mm × 5 mm size on it with a bridge pattern, which is suitable for resistivity measurements. Si substrates were then cleaned using a standard chemical cleaning process. Prior to deposition, these Si substrates were subjected to a glow discharge under high vacuum, so as to improve the Ni film to silicon wafer adhesion. Ni films with thicknesses, ranging from 7.0 to 89 nm were then deposited on Si substrate at 295 K by thermal evaporation. The thicknesses of the Ni films were determined by a quartz crystal oscillator with an accuracy of ±0.1 nm during the deposition.

Secondly, in order to form nickel di-silicide, Ni films were annealed by RTA process under pure and dry nitrogen ambient for 60 s at 850 °C. It has been found that annealing at 850 °C results in a significant increase in the thickness of the Ni films (about 4–6 times) and yields nickel di-silicide ($NiSi_2$) films with thicknesses ranging from 37 to 400 nm. The total thickness of the Ni–Si silicide films was determined using Rutherford back scattering spectrometry (RBS), cross-sectional SEM (X-SEM) and electrical sheet resistance measurements. Both thicknesses of the Ni–Si silicide films formed at 850 °C and as-deposited Ni films were listed in Table 1.

After RTA process, the sheet resistances of the Ni–Si silicide films formed at 850 °C were measured with a four-point probe technique with an accuracy of 0.2%. The structural analysis of the 850 °C-annealed Ni films was then performed using X-ray diffraction (XRD), Rutherford back scattering spectrometry (RBS), scanning electron microscopy (SEM and X-SEM) and atomic force microscopy (AFM).

XRD measurements were carried out using the Philips X'Pert Pro X-ray diffractometer with Cu Kα line for the identification of crystallographic phases and their grain sizes. RBS was used for the determination of layer thicknesses, elemental distribution and depth profiling. RBS measurements were carried out using 2.1 MeV He^+ ions in an IBM scattering geometry with particle detector placed at 170° from the incident beam. The RUMP simulation software [31,32] was used to analyze the RBS data in order to extract the silicide film thickness and stoichiometry. SEM measurements were carried out using the Philips XL-30S FEG scanning electron microscope. SEM and cross-sectional SEM (X-SEM) experiments were also employed to study either free surface or interfacial reactions and to determine the thicknesses of the silicide layers, respectively. AFM studies were performed using Nanoscope IV digital instrument to investigate the surface morphology of the Ni–Si silicide films.

3. Results and discussion

3.1. XRD measurements

XRD spectra of the Ni–Si films annealed at 850 °C is shown in Fig. 1 as a function of the selected films of 400, 170, 80 and 42 nm thickness. As seen from Fig. 1, the Si(4 0 0) peak observed at $2\theta \cong 69.15°$ is the main peak of Si(1 0 0) substrate. Si(2 0 0) peak at $2\theta \cong 33°$ is an additional peak which has been observed on almost all the Si(1 0 0) substrates. Apart from this the peak observed at $2\theta \cong 61.7°$ belongs to the Cu Kβ radiation diffracted from the Si(4 0 0) planes. The peaks seen at $2\theta \cong 27°$, $2\theta \cong 33°$ and $2\theta \cong 47°$ belong to $NiSi_2$(1 1 1), $NiSi_2$(2 0 0) and NiSi(2 1 1) phases, respectively. It is clearly seen from Fig. 1 that in the thickest Ni–Si film of 400 nm (sample 2′) apart from the Si peaks, the $NiSi_2$(1 1 1), $NiSi_2$(2 0 0) di-silicide phases and NiSi(2 1 1) nickel mono-silicide phase are also formed, signaling the complete conversion of Ni overlayer to final $NiSi_2$ and intermediate NiSi phases. In addition $NiSi_2$(2 0 0) di-silicide phase seems to be superposed with Si(2 0 0) peak at $2\theta \cong 33°$, because of the small difference in 2θ between $NiSi_2$(2 0 0) and Si(2 0 0) phases (the lattice mismatch between Si and $NiSi_2$ is only 0.4%) [20,23]. As the film thickness decreases from 400 to 170 nm, $NiSi_2$(1 1 1), $NiSi_2$(2 0 0) and NiSi(2 1 1) silicide phases are still present, however, the peak height of $NiSi_2$(1 1 1) phase decreases, whereas that of the $NiSi_2$(2 0 0) increases. As the film thickness decreases to ≤80 nm, both NiSi(2 1 1) and $NiSi_2$(1 1 1) peaks completely disappear, while relatively weak and broad

Table 1
The room temperature electrical sheet resistance, resistivity and grain size values of the Ni–Si silicide films formed by rapid thermal annealing (RTA) at 850 °C for 60 s, d_{Ni}: thickness of the as-deposited Ni film, d_{Ni-Si}: total thickness of the Ni–Si silicide film, $\bar{D}_f$: average grain size of the Ni–Si silicide film calculated from XRD analysis and R_s^{Ni-Si} and ρ_f^{Ni-Si}: total measured sheet resistance and resistivity of the Ni–Si silicide film, respectively.

Sample number	d_{Ni} (nm)	d_{Ni-Si} (nm)	$\bar{D}_f$ (nm)	R_s^{Ni-Si} (295 K) Ω/□	ρ_f^{Ni-Si} (295 K) (10^{-8} Ωm)
2′	89.0	400	58.00	1.890	75.72
5′	63.2	170	42.90	5.360	91.12
9′	46.5	162	42.37	5.440	88.15
1′	43.1	105	38.63	10.43	109.5
10′	20.7	80	36.98	15.18	121.4
3′	31.2	72	36.46	17.54	126.3
12′	31.8	60	35.67	23.40	140.4
11′	11.0	42	34.49	42.71	179.4
7′	7.00	37	34.16	53.73	198.8

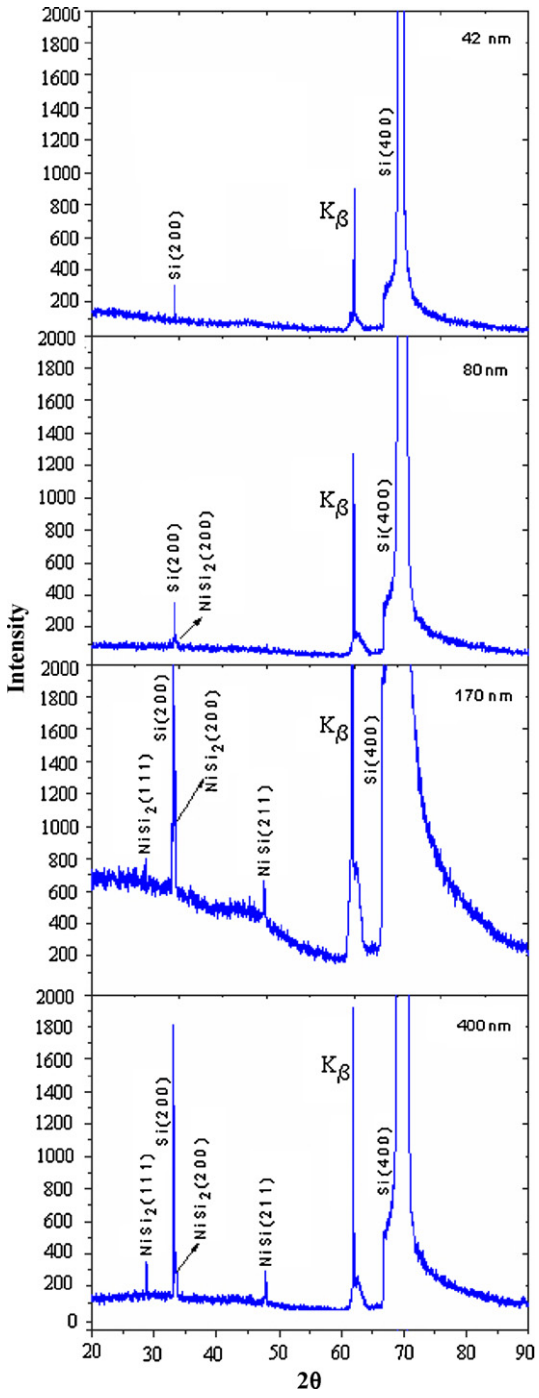

Fig. 1. XRD spectra of the Ni–Si silicide films formed by rapid thermal annealing (RTA) at 850 °C for 60 s, as a function of the selected films of 400, 170, 80 and 42 nm thickness, respectively. Both film thicknesses and NiSi, $NiSi_2$, Si peaks are marked.

$NiSi_2$(2 0 0) peak is observed. Finally for the thicknesses ≤80 nm, only Si peaks are visible in the XRD pattern.

3.2. RBS measurements

RBS spectrum and RUMP simulation of the Ni–Si silicide films of 400, 80 and 42 nm thickness are shown in Figs. 2–4, respectively. The tables of rump data of these samples are inserted into Figs. 2–4, respectively. As can be clearly seen from Figs. 2–4 and Table 2, in the thickest Ni–Si silicide films of 400–170 nm, which have initial Ni film of 89–63.2 nm, most of the Ni:Si ratios are associated with

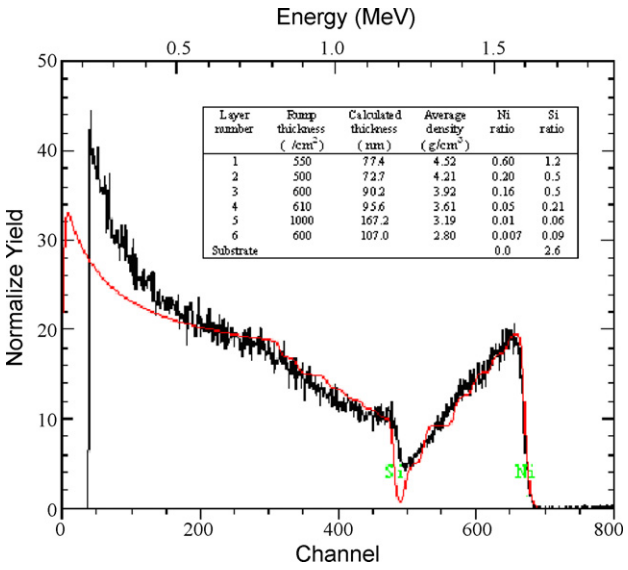

Layer number	Rump thickness (/cm²)	Calculated thickness (nm)	Average density (g/cm³)	Ni ratio	Si ratio
1	550	77.4	4.52	0.60	1.2
2	500	72.7	4.21	0.20	0.5
3	600	90.2	3.92	0.16	0.5
4	610	95.6	3.61	0.05	0.21
5	1000	167.2	3.19	0.01	0.06
6	600	107.0	2.80	0.007	0.09
Substrate				0.0	2.6

Fig. 2. RBS spectrum and RUMP simulation for Ni–Si silicide film of 400 nm thickness (sample 2′) formed by RTA at 850 °C for 60 s. The inset shows RUMP data of sample 2′.

$NiSi_2$ (nickel di-silicide), while for the thinner films of 80–42 nm with initial Ni films of 20–11 nm, the Ni:Si ratios belong to more and more Si-rich silicide phases. Based on our RBS analysis, we can conclude that the nucleation of $NiSi_2$ phase begins more easily either at even a lower temperature than 850 °C for 60 s or at even a lower annealing time than 60 s for 850 °C within thinner silicide films of 80–42 nm. Both Ni:Si ratios and the values of the density in the layers reveal a slightly higher amount of Si in the layers than those of stoichiometrically calculated values for silicide phases. This result can be explained by the fact that $NiSi_2$ phase may not be present as a layer but in the form of islands exposing the Si substrate region, which is consistent with the previous observations [6–10].

As can be seen from Table 2, there is also a good agreement between phases displayed by RBS and XRD spectrum except for Si-rich silicide phases, which cannot be observed by XRD. It should be noted that RBS can detect phases at deeper depths due to its depth-resolved capability, whereas XRD can probe near-surface

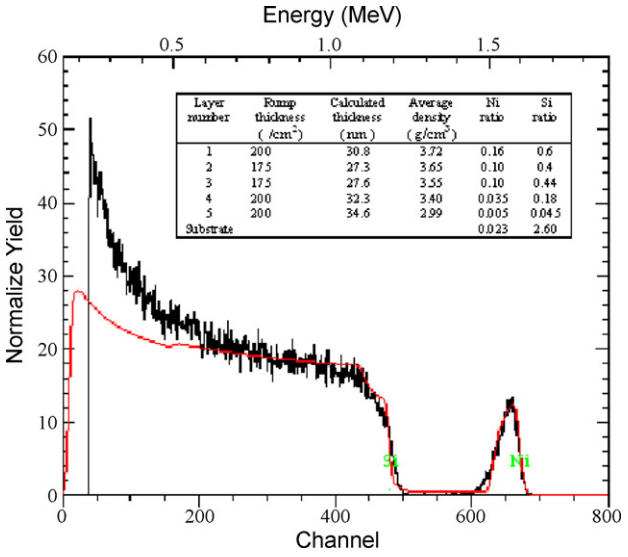

Layer number	Rump thickness (/cm²)	Calculated thickness (nm)	Average density (g/cm³)	Ni ratio	Si ratio
1	200	30.8	3.72	0.16	0.6
2	175	27.3	3.65	0.10	0.4
3	175	27.6	3.55	0.10	0.44
4	200	32.3	3.40	0.035	0.18
5	200	34.6	2.99	0.005	0.045
Substrate				0.023	2.60

Fig. 3. RBS spectrum and RUMP simulation for Ni–Si silicide film of 80 nm thickness (sample 10′) formed by RTA at 850 °C for 60 s. The inset shows RUMP data of sample 10′.

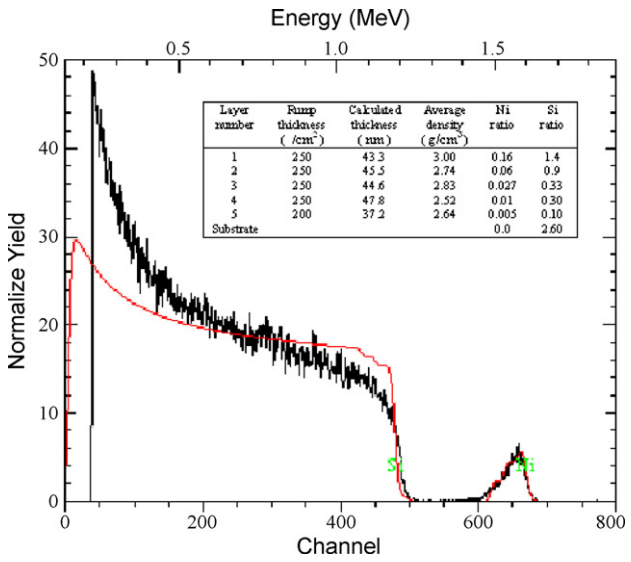

Fig. 4. RBS spectrum and RUMP simulation for Ni–Si silicide film of 42 nm thickness (sample 11′) formed by RTA at 850 °C for 60 s. The inset shows RUMP data of sample 11′.

regions. Therefore, Si-rich phases, formed at deeper depths near the interfacial regions cannot be detected by XRD.

The total film thickness of the Ni–Si silicide films of 850 °C has been calculated using three different techniques namely RBS, X-SEM and electrical sheet resistance measurements. In the sheet resistance measurement technique, we have determined the thicknesses of the silicide films in the usual way by comparing the measured resistance values (R) at 273 and 120 K of the silicide films with the measured resistivities ($\rho_{\infty}^{\mathrm{Ni-Si}}$) of the bulk Ni–Si silicide film at these temperatures, from the equation:

$$d_{\mathrm{Ni-Si}} = \frac{\ell}{b}\frac{\rho_{\infty}^{\mathrm{Ni-Si}}(273) - \rho_{\infty}^{\mathrm{Ni-Si}}(120)}{R(273) - R(120)}$$

where l and b are the length and the width of the Ni–Si silicide films, respectively. The thickness of two thickest Ni–Si silicide films (samples 2′ and 5′) are found to be 400 and 170 nm, respectively, with electrical sheet resistance measurements.

It should be pointed out that at thicknesses ≥80 nm each technique yield almost comparable thickness values, whereas at thicknesses ≤80 nm they are not able to yield comparable thickness values because of the formation of the Si-enriched silicide layers. In addition, corresponding to the thicknesses < 42 nm, the calculated thickness values from the sheet resistance measurements are considerably smaller than those obtained by RBS and X-SEM techniques. This result can be explained in terms of the occurrence of the more and more Si-rich layers ($NiSi_9$, $NiSi_{30}$, etc.), which are not able to contribute to the electrical conductivity. Our analysis shows that if these electrically dead Si-rich layers are disregarded, there is a good agreement between thickness values calculated by RBS and electrical resistivity measurements. Therefore, in this study the thickness values determined from electrical measurements are used as the effective film thickness for each sample studied.

3.3. SEM, X-SEM and AFM measurements

The SEM images obtained from Ni–Si silicide films formed at 850 °C are shown in Fig. 5 for selected films of 400, 170, 80 and 42 nm thickness. It is clearly evident from Fig. 5 that Ni–Si silicide films formed at 850 °C exhibit a considerably different polycrystalline film morphology with film thickness, viz., non-uniform, relatively large grains, accompanying with high roughness, high Si concentration and lattice defects. Pattern obtained from our thickest Ni–Si silicide film of 400 nm (sample 2′) exhibit a complex polycrystalline structure, consisting of large grains with well defined grain boundaries of relatively small voided regions of exposed Si, in which NiSi (bright-white) and $NiSi_2$ (dark-grey) phases co-exist. Corresponding to this sample, our XRD analysis yields an average grain size, D = 58.0 nm for the film (Table 1) and an average grain size values of 62.1, 42.1 and 53.0 nm for $NiSi_2$(1 1 1), $NiSi_2$(2 0 0) and NiSi(2 1 1) phases (Table 2). In the case of the Ni–Si silicide film of 170 nm (sample 5′) these large grains for co-existence of $NiSi_2$ and NiSi are separated from one another by well defined grain boundaries, with relatively large voided regions of exposed Si. These grain boundaries are characterized by holes. As seen clearly from Fig. 5a and b, NiSi phase (bright-white) seems to be distributed uniformly on the boundaries of $NiSi_2$ grains and can also be observed in Si matrix (dark phases). These experimental results clearly reveal that there is island growth of $NiSi_2$ in NiSi matrix, in accordance with the earlier observations [6,7,25,33]. Julies et al. [6] have reported through TEM and SEM measurements that the NiSi phase was stable up to about 700 °C and at about 750 °C NiSi reacted with the silicon substrate to form $NiSi_2$, which seems to grow as islands in a NiSi matrix, revealing the possible growth of $NiSi_2$ at the expense of NiSi grains.

Our SEM measurements also show that as the film thickness decreases from 400 to 170 nm, $NiSi_2$ grains co-existing with NiSi start to agglomerate and become smaller in size where XRD analysis yields an average grain sizes 31.8, 35.3 and 27.1 nm for $NiSi_2$(1 1 1), $NiSi_2$(2 0 0) and NiSi(2 1 1) phases, respectively (Table 2), while the voided regions of exposed Si (or holes) become larger. As seen from Fig. 5c and d, for the film of 80 nm, these holes seem to coalesce into larger ones and finally at thicknesses ≤42 nm some holes on the

Table 2
Comparison of different silicide phases identified using RBS and XRD for the Ni–Si silicide films formed by rapid thermal annealing (RTA) at 850 °C for 60 s, $d_{\mathrm{Ni-Si}}$: total thickness of the Ni–Si silicide film and $\bar{D}$: average grain size of the silicide phases calculated from XRD analysis.

$d_{\mathrm{Ni-Si}}$ (nm)	Silicide composition		
	RBS	XRD	$\bar{D}$ (nm)
400	$NiSi_2$, Si-rich phases ($NiSi_3$–$NiSi_{13}$)	$NiSi_2$(1 1 1) $NiSi_2$(2 0 0) NiSi(2 1 1) Si peaks	62.1 42.1 53.0 –
170	$NiSi_2$, Si-rich phases ($NiSi_3$–$NiSi_{13}$)	$NiSi_2$(1 1 1) $NiSi_2$(2 0 0) NiSi(2 1 1) Si peaks	31.8 35.3 27.1 –
80	Si-rich phases ($NiSi_3$–$NiSi_9$)	$NiSi_2$(2 0 0) (very weak) Si peaks	30.1 –
42	Si-rich phases ($NiSi_9$–$NiSi_{30}$)	Si peaks	–

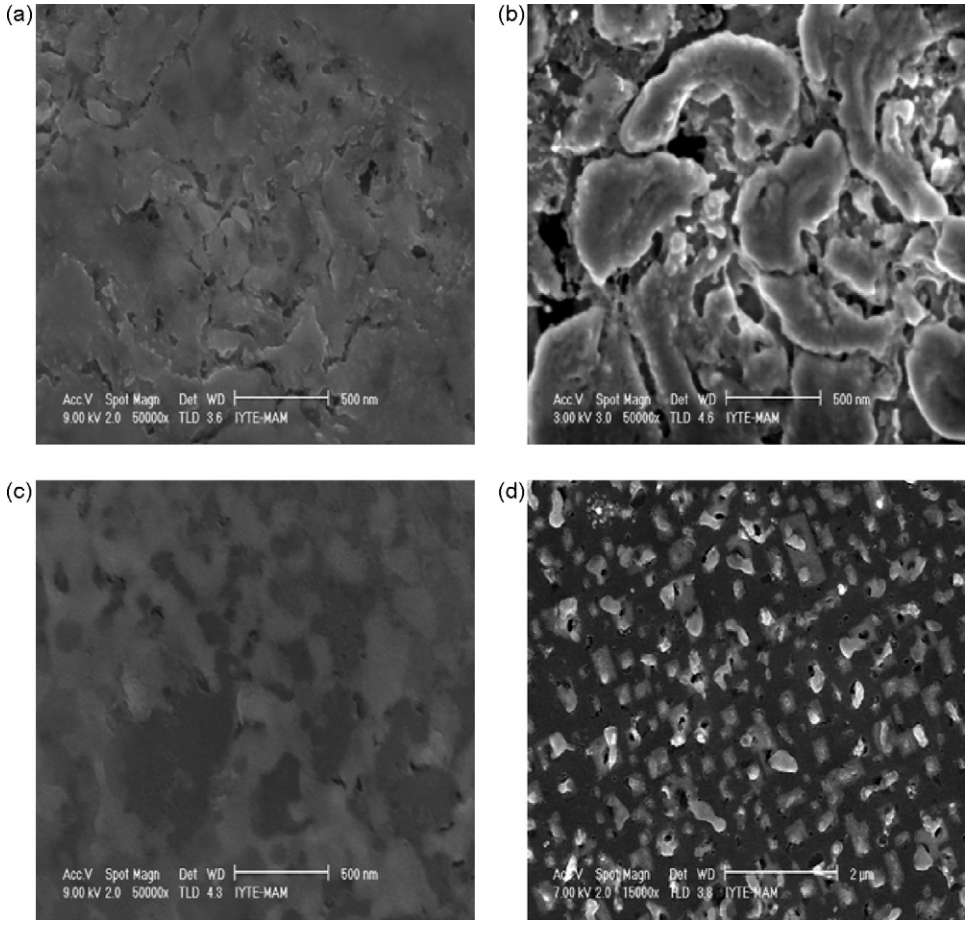

Fig. 5. SEM micrographs of the Ni–Si silicide films formed by RTA at 850 °C for 60 s, as function of the selected films with thicknesses (a) 400 nm, (b) 170 nm, (c) 80 nm and (d) 42 nm. The bright-white, dark-grey and dark phases represent NiSi, $NiSi_2$ and Si, respectively.

grain boundaries even grow in size until a visible (or continuous) hole exists from the top of the Si-rich silicide islands to the silicon substrate. In addition Si-enriched silicide islands with visible hole seems to precipitate finely in Si matrix. In other words, for the films with thicknesses ≤80 nm, $NiSi_2$ agglomeration is accompanied with grain boundary grooving, followed by grain separation and formation of Si-rich silicide islands, resulting in a dramatic increase in sheet resistance in accordance with grain grooving model [24–27]. Therefore, thermal stability (or quality) of these films considerably degrades due to both substantial increase in Si concentration and the occurrence of the silicide islands with small visible holes, yielding a remarkable increase in sheet resistance values of the Ni–Si films thinner than 80 nm. It is also very clear from these experimental results that thinner films with thicknesses ≤80 nm are thermally less stable than thicker films of 400–105 nm and $NiSi_2$ agglomeration occurs at a lower temperature than both 850 °C and normally expected value of 1000 °C for $NiSi_2$ phase [25,28]. Therefore, in order to delay the $NiSi_2$ agglomeration, accompanied with grain boundary grooving, followed by grain separation and Si-rich silicide island formation, annealing temperature and/or annealing time should be fixed at <850 °C and at <60 s, respectively, for the Ni–Si films with thicknesses ≤ 42 nm.

Fig. 6 shows the silicide/Si interface morphology obtained from the cross-sectional SEM (X-SEM) study for the silicide films of 170 nm (sample 5′). The X-SEM micrograph of the sample 5′ reveals a relatively rough silicide/Si interface which suggests that NiSi agglomeration is progressed considerably so as to transform into $NiSi_2$. In addition the existence of the relatively rough silicide/Si interface consisting of adjacent NiSi/Si and $NiSi_2$/Si interfaces clearly indicate the possible growth of $NiSi_2$ at the expense of NiSi grains, which is consistent with the earlier observations [6,7].

AFM images of the Ni–Si films of 170 nm clearly reveal that the pillar-like structure of NiSi phase coalesces so as to form a ridge-like structure for the $NiSi_2$ phase, which is consistent with previous observations [18,25,33]. For the films with thicknesses ≤170 nm the ridge-like structure for $NiSi_2$ phase shows a general trend of decreasing average diameter and mean roughness values, with decreasing film thickness. Based on the AFM analysis

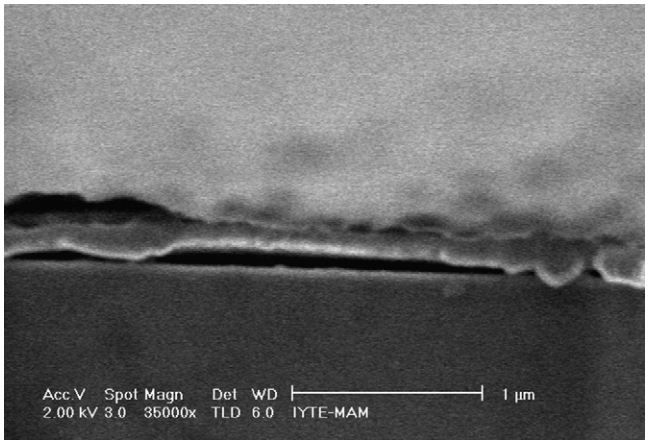

Fig. 6. X-SEM image showing silicide/Si interface morphology of the Ni–Si silicide film of 170 nm thickness (sample 5′) formed by RTA at 850 °C for 60 s.

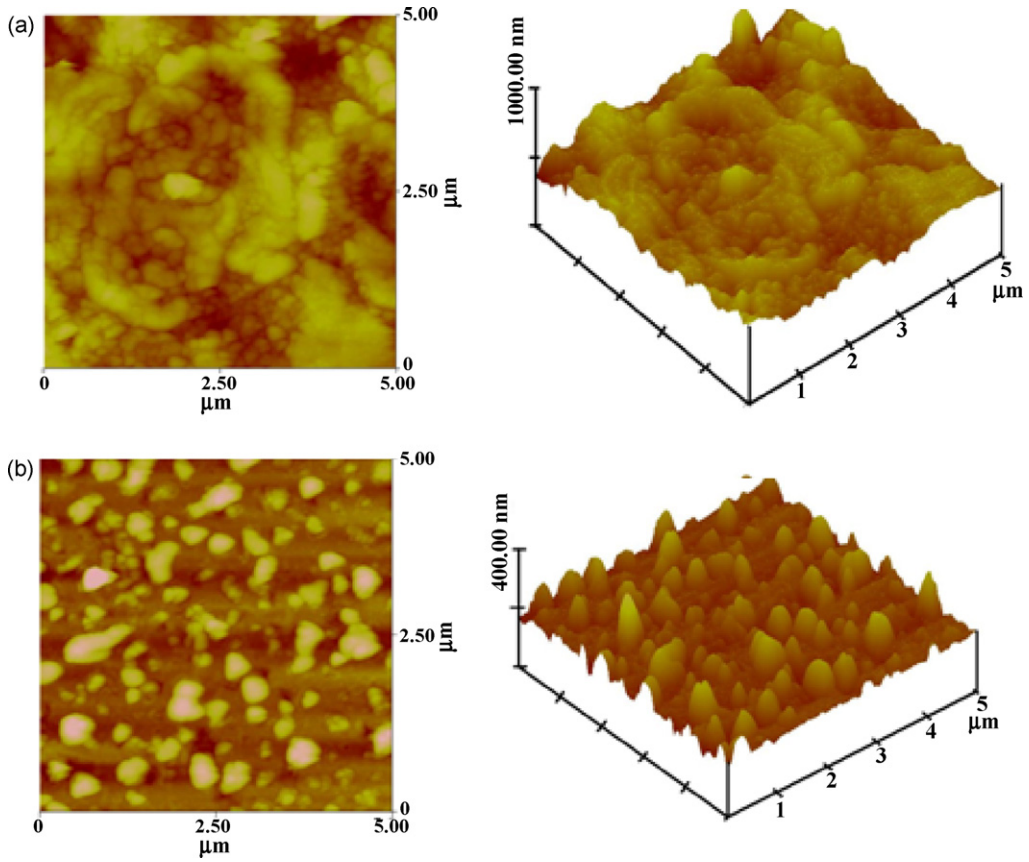

Fig. 7. AFM images of the Ni–Si silicide films formed by RTA at 850 °C for 60 s, as a function of the selected films with thickness (a) 170 nm (sample 5′) and (b) 42 nm (sample 11′).

shown in Fig. 7a and b, as the film thickness decreases from 170 to 42 nm, the average grain diameter of the Ni–Si films decreases from 43 to 35 nm. The mean roughness values corresponding to the film agglomeration also decreases 38–20 nm (about 2 times) due to the phase transformation from the $NiSi_2$-rich silicide phases to the island-like Si-rich silicide phases. Over the thickness range of 80–42 nm, irregular $NiSi_2$ grains further groove laterally, resulting in Si-enriched silicide grains grown more epitaxially at the expense of the adjacent unconverted $NiSi_2$ grains. The occurrence of the more epitaxial Si-rich silicide islands with visible hole results a significant decrease in the mean roughness values from 38 to 20 nm (about 2 times), while a remarkable increase in sheet resistance from 1.89 to 53.73 Ω/□. These results also clearly indicates that the Si-enriched island-like Ni–Si silicide films with thickness <42 nm are thermally less stable than the thickest films of 400–105 nm.

3.4. Electrical sheet resistance measurements

For the room temperature (at 295 K), the measured electrical sheet resistance, resistivity and grain size values of the Ni–Si silicide films of 400–37 nm thicknesses are listed in Table 1. Fig. 8 shows the variation of sheet resistance of the Ni–Si silicide films as function of the silicide film thickness. As is clearly seen from both Table 1 and Fig. 8, the sheet resistance of the Ni–Si silicide films increases significantly with decreasing silicide film thickness. This result clearly indicate that the sheet resistance of the Ni/Si samples is significantly dependent on the silicide film thickness via initial Ni film thickness, due to the Ni/Si concentration ratio available for the Ni–Si silicide phase formation for a given annealing temperature.

So as to establish a correlation between the developed phases and sheet resistances of the Ni–Si films, we can classify our silicide samples into three groups by taking into account their phases, the thickest ones with thickness of 400–162 nm, the relatively thinner ones with thickness of 105–80 nm and the thinnest ones of 42–37 nm, respectively. As can be seen from Table 1, the thickest Ni–Si silicide films of 400–162 nm have sheet resistances, varying from 1.89 to 5.44 Ω/□, while the thinner silicide films of 105–70 nm exhibit sheet resistances between 10.43 and 15.18 Ω/□ (about 2 times that of the first group films) and thinnest films with 42–37 nm show a considerable high sheet resistance ranging from 42.71 to

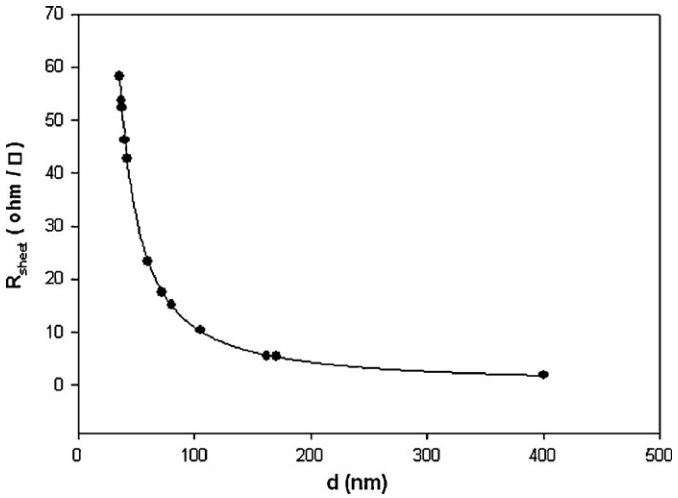

Fig. 8. The variation of the sheet resistance of the Ni–Si silicide films formed by RTA at 850 °C for 60 s as a function of the silicide film thickness.

53.73 Ω/□ (about 5 and 10–20 times those of the thinner and thickest ones, respectively). Assuming no agglomeration in $NiSi_2$ phase, the expected sheet resistance is found to be 7.84 Ω/□ for $NiSi_2$ from the reference data in Ref. [23]. Based on above discussion, for the thickest films of 400–162 nm, with initial Ni films of 89–46.5 nm, which have $R_s \leq 5.44\,\Omega/\square$, the observed slight sheet resistance increase with decreasing film thickness should be a result of the slow conversion of NiSi to irregular nucleation of $NiSi_2$, resulting co-existence of NiSi and $NiSi_2$ phases rather than the film agglomeration. Whereas, the higher sheet resistances of the thinner samples of 105–70 nm (with initial Ni films of 43.1–31.8 nm), should be related to the gradual increase in the $NiSi_2$ agglomeration due to the occurrence of the Si-rich silicide phases. For the thinnest films of 42–37 nm (with initial Ni films of 11–7 nm), the observed remarkable sheet resistance increase (ranging from 42.71 to 53.73 Ω/□) should be caused by the substantial agglomeration of the $NiSi_2$ phase, resulting in grain separation and formation of Si-enriched silicide islands with visible holes, as a result of the substantial enlargement in area fraction of Si in the lattice. This indicates that the Si-enriched Ni–Si silicide films with thicknesses ≤80 nm are thermally unstable, whereas thickest films of 400–105 nm thickness present better thermal stability than the thinnest ones in terms of both agglomeration and phase transformation, which is consistent with earlier studies [25].

4. Conclusions

In this study, XRD and RBS analysis have revealed that in the Ni–Si silicide films of 400–105 nm thickness, NiSi and $NiSi_2$ silicide phases co-exist, indicating that Ni overlayer is completely transformed to intermediate NiSi and final $NiSi_2$ silicide phases. In addition the peak height of NiSi(2 1 1) and $NiSi_2$(2 0 0) phases both increase, while that of the $NiSi_2$(1 1 1) decreases with decreasing film thickness over the thickness range of 400–105 nm. At thicknesses ≤ 80 nm, these silicide phases completely disappear, but more and more Si-rich silicide phases are formed.

Apart from this, SEM measurements reveal that over the thickness range of 400–170 nm, Ni–Si silicide films consist of relatively large grains for co-existence of $NiSi_2$ and NiSi phases which are separated from one another by large voided regions of exposed Si characterized by 'holes'. This indicate that $NiSi_2$ grow as islands in NiSi matrix. These silicide films of 400–170 nm have sheet resistances, ranging from 1.89 to 5.44 Ω/□ and good thermal stability in terms of both agglomeration and phase transformation. As the film thickness decreases from 170 to 42 nm, NiSi and $NiSi_2$ grains becomes smaller, while dark phases (or holes) on the grain boundaries grow even larger. As evidenced by RBS and SEM for the thicknesses ≤ 42 nm, Si-enriched silicide islands with visible holes seems to precipitate finely in Si matrix, resulting in a remarkable high sheet resistance values ranging from 42.71 to 53.73 Ω/□. Therefore, the silicide films with thicknesses ≤ 80 nm present worse thermal stability than the thickest ones in terms of both agglomeration and phase transformation.

The combination of our sheet resistance and structural measurements shows that as the silicide film thickness decreases from 400 to 37 nm (or as the initial Ni film thickness decreases from 89 to 7 nm), the observed dramatic sheet resistance increase is generated by substantial $NiSi_2$ phase agglomeration, accompanied by grain boundary grooving, followed by silicide island formation.

Acknowledgements

The authors wish to express their appreciation for the use of the facilities at the Center for Irradiation of Materials, Alabama A&M University and the Institute of Science and Technology.

References

[1] S.P. Murarka, Silicides for VLSI Application, Academic, New York, 1983.
[2] M.A. Nicolet, S.S. Lau, in: N.G. Einspruch (Ed.), VLSI Electronic Microstructures Science, vol. 6, Academic Press, New York, 1983.
[3] Y. Hu, S.P. Tay, J. Vac. Sci. Technol. A 16 (1998) 1820.
[4] A.H. Reader, A.H. van Ommen, P.J.W. Weijs, R.A.M. Wolters, D.J. Oostra, Rep. Prog. Phys. 56 (1992) 1397.
[5] J.P. Gambino, E.G. Colgan, Mater. Chem. Phys. 52 (1998) 99.
[6] B.A. Julies, D. Knoesen, R. Pretorius, D. Adams, Thin Solid Films 347 (1999) 201.
[7] S. Abhaya, G. Amarendra, S. Kalavathi, P. Gopalan, M. Kamruddin, A.K. Tyagi, V.S. Sastry, C.S. Sundar, Appl. Surf. Sci. 253 (2007) 3799.
[8] D. Ma, D.Z. Chi, M.E. Loomans, W.D. Wang, A.S.W. Wong, S.J. Chua, Acta Mater. 54 (2006) 4905.
[9] S.Y. Tan, C.-W. Chen, I.-T. Chen, C.-W. Feng, Thin Solid Films 517 (2008) 1186.
[10] M. Tinani, A. Mueller, Y. Gao, E.A. Irene, J. Vac. Sci. Technol. B 19 (2001) 376.
[11] M. Bhaskaran, S. Sriram, T.S. Perova, V. Ermakov, G.J. Thorogood, K.T. Short, A.S. Holland, Micron 40 (2009) 89.
[12] O. Song, D. Kim, C.S. Yoon, C.K. Kim, Mater. Sci. Semicond. Process. 8 (2005) 608.
[13] L.A. Clevenger, C.V. Thomson, K.N. Tu, J. Appl. Phys. 67 (1990) 2894.
[14] G.B. Kim, D.-J. Yoo, H.K. Baik, J.-M. Myoung, S.M. Lee, S.H. Oh, C.G. Park, J. Vac. Sci. Technol. B 21 (2003) 1319.
[15] H.N. Zhu, B.X. Liu, Surf. Coat. Technol. 131 (2000) 307.
[16] B.X. Liu, K.Y. Gao, H.N. Zhu, J. Vac. Sci. Technol. 17 (1999) 2277.
[17] D.H. Zhu, K. Tao, F. Pan, B.X. Liu, Appl. Phys. Lett. 62 (1993) 2359.
[18] S. Abhaya, G. Amarendra, G.L.N. Padma Gopalan, S. Reddy, Saroja, J. Phys. D: Appl. Phys. 37 (2004) 3140.
[19] J.W. Mayer, J.M. Poate, in: J.M. Poate, K.N. Tu, J.W. Mayer (Eds.), Thin Films Interdiffusion and Reactions, Wiley, New York, 1978, p. 359.
[20] F. Deng, R.A. Johnson, P.M. Asbeck, S.S. Lau, W.B. Dubbelday, T. Hsiao, J. Woo, J. Appl. Phys. 81 (1997) 8047.
[21] K.N. Tu, E.I. Alessandrini, W.K. Chu, H. Krautle, J.W. Mayer, Jpn. J. Appl. Phys. 2 (1974) 669.
[22] Pourtois, C. Demeurisse, T. Schram, B. Brijs, M. De Potter, C. Vrancken, K. Maex, Microelectr. Eng. 82 (2005) 441.
[23] K. Maex, M. Van Rossum, Properties of Metal Silicides, INSPEC, London, 1995.
[24] D.-X. Xu, S.R. Das, C.J. Peters, L.E. Erickson, Thin Solid Films 326 (1998) 143.
[25] F.F. Zhao, J.Z. Zheng, Z.X. Shen, T. Osipowicz, W.Z. Gao, L.H. Chan, Microelectr. Eng. 71 (2004) 104.
[26] W.W. Mullins, J. Appl. Phys. 28 (1957) 333.
[27] H. Jeon, C.A. Sukow, J.W. Honeycutt, G.A. Rozgonyi, R.J. Nemanich, J. Appl. Phys. 71 (1992) 4269.
[28] L. Ehouarne, M. Putero, D. Mangelinck, F. Nemouchi, T. Bigault, E. Ziegler, R. Coppard, Microelectr. Eng. 83 (2006) 2253.
[29] F. Nemouchi, D. Mangelinck, C. Bergman, P. Gas, Appl. Phys. Lett. 86 (2005) 041903.
[30] C. Lavoie, et al., Microelectr. Eng. 70 (2003) 144.
[31] S. Budak, C. Muntele, I. Muntele, H. Guo, A. Gupta, D. Ila, Nucl. Instrum. Methods Phys. Res. B 261 (2007) 686.
[32] L.R. Doolittle, M.O. Thompson, RUMP, Computer Graphics Service, 2002.
[33] S. Ilango, G. Raghavan, M. Kamruddin, S. Bera, A.K. Tyagi, Appl. Phys. Lett. 87 (2005) 101911.